MCB
Journals.ASM.org

Selective Inhibition of Hypoxia-Inducible Factor 1α Ameliorates Adipose Tissue Dysfunction

Kai Sun,[a] Nils Halberg,[a]* Mahmood Khan,[b] Ulysses J. Magalang,[c] Philipp E. Scherer[a,d]

Touchstone Diabetes Center, Departments of Internal Medicine[a] and Cell Biology,[d] University of Texas Southwestern Medical Center, Dallas, Texas, USA; Division of Cardiovascular Medicine[b] and Division of Pulmonary, Allergy, Critical Care and Sleep Medicine,[c] Wexner Medical Center, The Ohio State University, Columbus, Ohio, USA

Hypoxia-inducible factor 1α (HIF1α) induction in adipocytes is a critical component of the "fibrotic response," directly linked to metabolic dysfunction in adipose tissues under hypoxic conditions. We reasoned that inhibition of HIF1α may ameliorate the negative aspects of the obesity-associated fat pad expansion. We used the selective HIF1α inhibitor PX-478, whose effectiveness has previously been established in tumor models. We demonstrate that PX-478 treatment effectively suppresses the high-fat-diet (HFD)-induced HIF1α activation in adipose tissue. HIF1α inhibition causes a reduction of weight gain in mice on an HFD but not on a chow diet. Treatment increases energy expenditure and prompts resistance to HFD-mediated deterioration of metabolic parameters. Moreover, PX-478-treated mice have reduced fibrosis and fewer inflammatory infiltrates in their adipose tissues. We confirm the metabolic effects obtained with PX-478 treatment using an adipose tissue-specific, doxycycline-inducible dominant negative HIF1α mutant (dn-HIF1α). Consistent with the pharmacological results, genetic inhibition of endogenous HIF1α activity prompts similar metabolic improvements in HFD-fed mice. Collectively, our results demonstrate that HIF1α inhibition in the adipocyte leads to significant metabolic improvements, suggesting that selective HIF1α inhibition in adipose tissue may be an effective therapeutic avenue in the context of metabolic dysfunction.

The overall metabolic health of an entire organism depends on how well adipose tissue copes with excessive caloric intake (1). To accommodate excess lipids, adipose tissue can undergo massive expansion by hypertrophy and hyperplasia (2, 3). Due to an underdeveloped vascular system, this expansion leads to the shortage of oxygen, and overnutrition leads very quickly to an acute, intermittent and eventually chronic condition of hypoxia in adipose tissue (4–6). Prevailing high levels of hypoxia in white adipose tissues (WATs) has been demonstrated in many obese rodent models and very reproducibly in human obese adipose tissue as well, though to a smaller extent (4, 6–9). Notably, these hypoxic conditions are most prominent in adipose tissues and are not observed in other tissues.

The transcription factor hypoxia-inducible factor 1 (HIF1), the key regulator of many cellular antihypoxic responses, is induced as an adaptive response to adipose tissue hypoxia (4, 9–11). HIF1 is a heterodimer consisting of HIF1α and HIF1β (12). HIF1β is constitutively expressed, and its levels are not regulated by hypoxia (12); in contrast, HIF1α induction is functionally more rate limiting (13). Even though it is also constitutively expressed, HIF1α is highly prone to ubiquitination and is rapidly degraded in the presence of oxygen (14). However, under hypoxic conditions, HIF1α is stabilized, and the accumulated protein quickly translocates into the nucleus, where it forms heterodimeric complexes with HIF1β (15–17). The heterodimers bind to genomic hypoxia response elements (HREs) and transactivate a wide variety of genes, including genes whose protein products are involved in cell survival, glycolysis, erythropoiesis, and angiogenesis (18, 19). However, in contrast to its function in many other tissues, HIF1α does not induce a proangiogenic response in adipose tissue, even if provided in excess (10). Instead, a transcriptional program is induced that entails a comprehensive induction of extracellular matrix components (ECM), ultimately leading to extensive tissue fibrosis (10, 20). This abnormal accumulation of ECM further causes an infiltration of inflammatory cells, which ultimately leads to a pattern of dysfunctional adipose tissue and an unfavorable metabolic profile (1).

Due to its essential roles in tumor progression, many strategies have been applied to target HIF1α directly in cancer therapies (21, 22). While natural antagonists, such as p35srj, or antisense strategies have been applied in mouse models, therapeutic strategies have mainly focused on developing novel small-molecule HIF1α inhibitors (23–25). By screening an extensive small-compound library, Welsh and colleagues identified a selective HIF1α inhibitor and named it PX-478 {*S*-2-amino-3-3[4′-*N*,*N*,-bis(2-chloroethyl)amino]phenyl propionic acid *N*-oxide dihydrochloride} (26). Experiments in different cancer models suggest that PX-478 bears promise for curbing the growth of a number of different tumors (26–33). While the detailed mechanism of action remains unclear, PX-478 inhibits HIF1α at multiple levels (26, 29): It decreases HIF1α mRNA levels; it blocks HIF1α translation, and it inhibits HIF1α deubiquitination, consequently leading to an increased ubiquitination of HIF1α and enhanced degradation. All these processes are independent of pVHL (the von Hippel-Lindau tumor suppressor protein) or p53.

Another method to target HIF1α is through genetic disruption

Received 14 July 2012 Returned for modification 20 August 2012
Accepted 11 December 2012

Published ahead of print 17 December 2012

Address correspondence to Philipp E. Scherer, Philipp.Scherer@utsouthwestern.edu.

* Present address: Nils Halberg, Laboratory of Systems Cancer Biology, Rockefeller University, New York, NY, USA.

Supplemental material for this article may be found at http://dx.doi.org/10.1128/MCB.00951-12.

doi:10.1128/MCB.00951-12

of the endogenous protein. A dominant negative form (dn-HIF1α) lacking the DNA-binding domain, the transactivation domain, and the oxygen-dependent degradation domain of HIF1α has been reported to effectively disrupt HIF1α action and block its transactivation in different tissues, including neuronal cells and pancreatic cancer cells (34, 35). Specifically, the disruption of the HIF1pathways by dn-HIF1α abrogates glucose uptake and glycolysis, even though the proangiogenic response in these tissues is not affected (34). As a result, pancreatic cancer cells expressing dn-HIF1α show a reduced proliferation rate. Due to its dramatic effects on suppressing cancer cell growth (36, 37), inhibition of HIF1α action by dn-HIF1α has been considered a potential tool for the treatment of pancreatic cancers (34).

Despite extensive efforts to develop improved strategies to target HIF1α for cancer therapies and despite many studies suggesting that obese adipose tissue induces HIF1α (38), there have been no attempts to apply these strategies to treat obesity-related diseases. In this study, by using both pharmacological (PX-478) and genetic (dn-HIF1α) methods, we sought to determine whether HIF1α inhibition can improve metabolic function in obesity-related diseases. We demonstrate that by the two methods, mice exhibit similar metabolically beneficial phenotypes, including a decrease in body weight gain, improved insulin sensitivity, and overall metabolically more functional adipose tissue. Our results highlight the reduction of HIF1α activity as a potential therapeutic strategy to counteract obesity-related metabolic disorders, particularly if we managed to target adipose tissue relatively selectively.

MATERIALS AND METHODS

Animals. To generate a doxycycline (DOX)-inducible dn-HIF1α overexpression mouse model (TRE-dn-HIF1α), the cDNA for dn-HIF1α (amino acids 30 to ~389) (34, 35), lacking the region encoding the DNA-binding domain, the transactivation domain, and the oxygen-dependent degradation domain of HIF1α, was engineered into the pTRE-tight vector (Clontech). The rabbit β-globin 3′ untranslated region (UTR) was introduced into the vector to better stabilize the transcript and enhance the translation (39). After linearization, TRE-dn-HIF1α DNA was injected to embryos into a pure C57BL/6 background by the Transgenic Core Facility at the University of Texas Southwestern Medical Center. Adiponectin promoter driven-rtTA transgenic mice (Apn-rtTA) were on a pure C57BL/6 background and have previously been described (40). The characterization of the adiponectin promoter as a transgenic cassette has been described elsewhere (40). These mice were crossed with TRE-dn-HIF1α mice to generate the adipose tissue-specific DOX-inducible dn-HIF1α transgenic mice. All experiments were conducted using double transgenic Apn-rtTA and TRE-dn-HIF1α mice. All experiments were conducted using littermate control male mice and were started when they were 5 weeks old. Mice were housed in cages with a 12-h dark-light cycle and with free access to water and a regular chow diet (catalog number 5080; Labdiet). All animal studies were reviewed and approved by the Institutional Animal Care and Use Committee of University of Texas Southwestern Medical Center and The Ohio State University. For all the high-fat-diet (HFD) feeding experiments, mice were fed with a diet containing 60% of its calories from fat (catalog number D12492; Research Diets or Harlan, Madison, WI). The HFD paste with 600 mg DOX per 1 kg HFD also contained 60% of its calories from fat (catalog number S5867; Bio-Serv, Frenchtown, NJ).

Adipose tissue pO_2 measurement using EPR oximetry. Electron paramagnetic resonance (EPR) oximetry has been utilized to directly measure absolute values of partial oxygen pressure (pO_2) in intact biological tissue (41). EPR oximetry is minimally invasive and has high sensitivity and specificity to pO_2, and the probes are nontoxic, allowing for repeat measurements *in vivo* (42). We leveraged these advantages of EPR oximetry to directly measure adipose tissue pO_2 dynamically during HFD feeding. Six C57BL/6 wild-type male animals, 13 to 14 weeks of age, were used in this study. A small midline lower abdominal incision was made (under 2% isoflurane anesthesia) to expose one epididymal WAT (EWAT). Fifteen microliters of sonicated oxygen-sensing microcrystals of LiNc-BuO in saline (100 μg/ml) was injected into the middle of the EWAT using a 26-gauge needle. The sensitivity of the EPR line width of the LiNc-BuO probe to oxygen was calibrated as described previously (43). The animals were then placed in the L-band (~1.2 GHz) EPR spectrometer (Magnettech, Germany) with the EWAT and the gastrocnemius muscle placed adjacent to the loop of the surface coil resonator (Fig. 1A). The peak-to-peak line width was used to calculate the pO_2 using the standard calibration curve as previously described (44). The animals were then allowed to recover and fed an HFD for 8 to 10 weeks until a weight gain of approximately 10 g was achieved, at which time the EPR oximetry was repeated as described above. The animals were then sacrificed, and the EWAT was harvested for histological confirmation of the LiNc-BuO microcrystal placement and fibrosis.

PX-478 and digoxin (HIF1α inhibitor) treatment. The HIF1α-specific inhibitor PX-478 compound was provided by Oncothyreon Inc. It has been shown to be orally available (26, 29). For the subacute experiments, 6-week-old male C57BL/6 mice were gastric gavaged with 5 mg/kg (of body weight) PX-478 in phosphate-buffered saline (PBS) or with PBS placebo every day for 3 days. For the subchronic studies, 6-week-old male C57BL/6 mice were gastric gavaged with 5 mg/kg of PX-478 in PBS or with PBS placebo every second day. The gavage began 2 weeks after the initial exposure to the HFD and continued for 12 days. A metabolic cage study was performed after the final PX-478 administration at day 12. For the chronic treatment, 6-week-old male C57BL/6 mice were gastric gavaged with 5 mg/kg of PX-478 in PBS or with PBS placebo every second day. The gavage began 2 weeks after the initial exposure to the HFD and continued for 50 days. Food intake and body weights were monitored throughout the time course. An oral glucose tolerance test (OGTT) and an insulin tolerance test (ITT) were performed after 5 weeks on the HFD. At day 50, the mice were fasted for 3 h and anesthetized with isoflurane. Tissues and sera were collected for further analyses.

The other HIF1α inhibitor, digoxin, was purchased from Sigma-Aldrich Corp. (St. Louis, MO). For the subchronic treatment, 6-week-old male C57BL/6 mice were injected intraperitoneally (i.p.) with 2 mg/kg of digoxin in PBS or with PBS placebo every day. The injection began 2 weeks after the initial exposure to the HFD and continued for 14 days. Food intake and body weights were monitored throughout the time course. An OGTT and an ITT were performed after 5 weeks on the HFD. At day 14, the mice were fasted for 3 h and anesthetized with isoflurane. Tissues and sera were collected for further analyses.

Total calories in excreta and indirect calorimetric measurements. Two weeks after PX-478 treatment or DOX induction, the mice from each group were separated as two individuals per cage. The excreta from each cage were collected, dried, and weighed on a daily basis for 3 days. The collected stools were then pooled, and ~1 g of stools from each cage was sent to Central Analytical Laboratory, Department of Poultry Science, University of Arkansas, for total calorie analysis.

For the metabolic cage studies, mice were housed individually in metabolic chambers and maintained on a 12-h dark-light cycle with lights on from 7:00 a.m. to 7:00 p.m. at room temperature (20°C to ~22°C). Metabolic profiles were obtained continuously using TSA metabolic chambers (TSA System, Germany) in an open-circuit indirect calorimetric system. All PX-478-treated mice and their littermate controls were fed the HFD and water *ad libitum*. All dn-HIF1α transgenic mice and their littermate controls were also provided with HFD paste containing 600 mg/kg of DOX and water *ad libitum*.

Histology. Adipose and liver tissues were excised and fixed in PBS-buffered 10% formalin for 2 days. Following paraffin embedding, the tissue sections were stained with hematoxylin and eosin (H&E) and Mas-

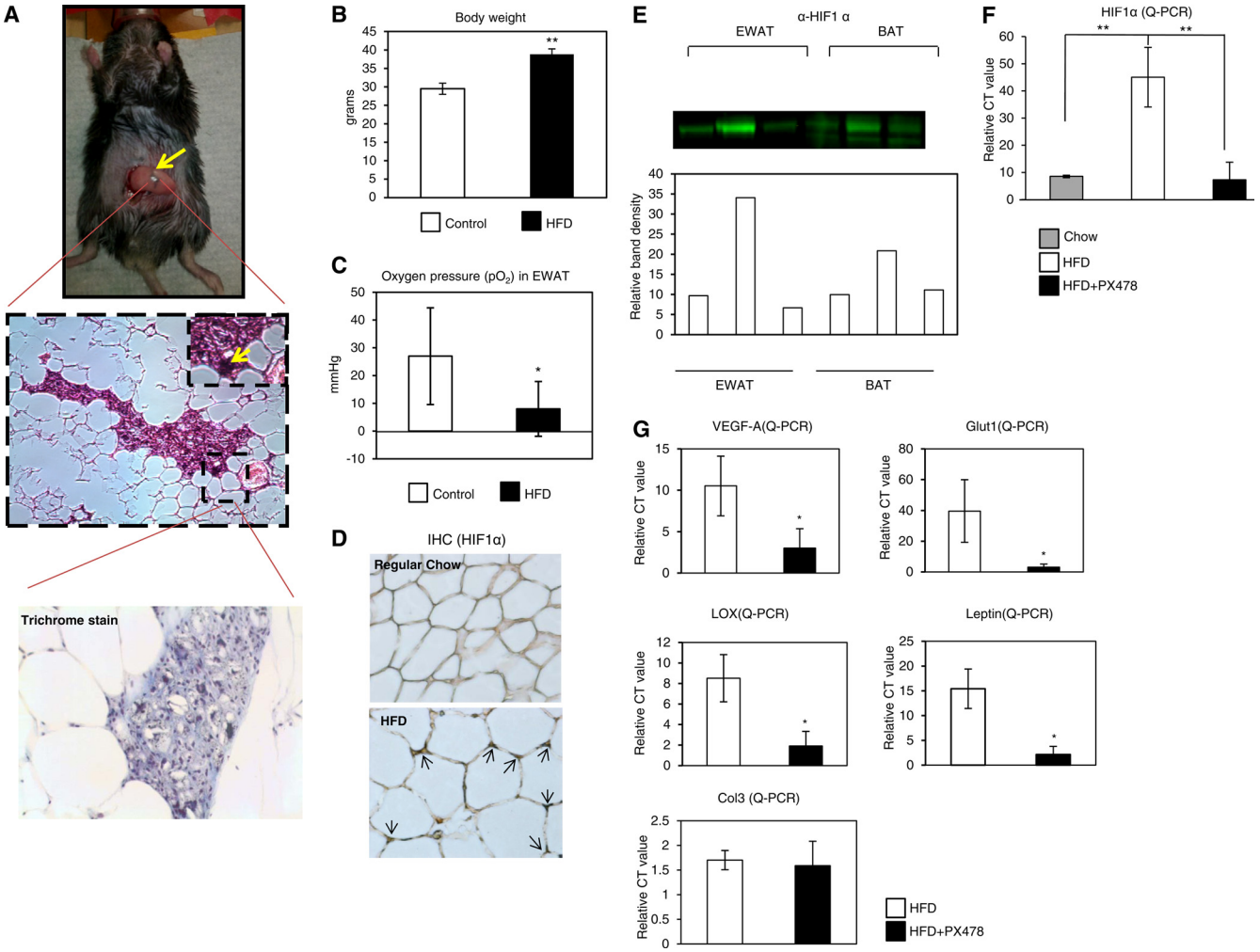

FIG 1 Detection of hypoxia, HIF1α induction in EWAT of HFD-fed mice, and PX-478-mediated suppression of the HFD-induced HIF1α. (A) (Top) To monitor the adipose tissue oxygen levels, the animal was under isoflurane inhalation anesthesia (2%) and then placed with the EWAT exposed to the loop of a surface-coil resonator. Sonicated oxygen-sensing microcrystals of LiNc-BuO were then implanted in the fat tissue for oxygen detection. The probe particulates are black, indicated by an arrow. (Middle) H&E staining of EWAT. The arrow indicates the EPR probes (tiny black crystals) in fat tissue. (Bottom) Trichrome staining of the location where the probe particulates were implanted in EWAT. Note the absence of fibrosis around the particles. (B) Baseline body weight (before starting the HFD feeding) and body weight after HFD feeding for 10 weeks ($n = 6$). C57BL/6 wild-type mice at 13 to 14 weeks of age were used in this study. The statistical significance was assessed by a Student t test. **, $P < 0.001$. (C) pO_2 measurements for the mice before and after HFD feeding by EPR spectrometer in the EWAT. The peak-to-peak line width was used to calculate the pO_2 using the standard calibration curve. *, $P < 0.05$. (D) Immunohistochemical staining by anti-HIF1α in EWAT of mice fed regular chow or an HFD. The arrows in the bottom image indicate upregulated HIF1α induced by the HFD. (E) Western blot analysis for HIF1α in EWAT and BAT of mice after 3-week feeding with chow, an HFD, and an HFD plus PX-478. Five mouse tissue samples were pooled for each well. The bottom portion shows quantitative measurements of the band density by ImageJ software from the NIH. (F) qPCR analysis of HIF1α in EWAT ($n = 5$ for each group). The readings are normalized by HPRT. **, $P < 0.001$. (G) qPCR analysis of HIF1α direct target genes in EWAT. *, $P < 0.05$.

son's trichrome using standard protocols. For immunohistochemistry (IHC), sections were deparaffinized. After antigen retrieval and blockage of endogenous peroxidase, sections were stained with primary antibodies against HIF1α (Novus Biologicals) or F4/80 (Santa Cruz) followed by biotinylated secondary antibodies (anti-mouse and anti-rabbit antibodies) (Dako, Glostrup, Denmark). Secondary antibodies were detected using a DAB chromogen A kit (Dako) by following the company's protocol. The slides were also counterstained with hematoxylin. All the images were acquired with Coolscope microscopy (Nikon). Quantification of adipocyte diameters was done on H&E-stained sections by the ImageJ software from the NIH.

Liver lipid content. Frozen liver tissues were used for lipid extraction and measurement by the UTSW Metabolic Core Facility. In brief, ~100- to 150-mg liver chunks were stored frozen until analysis. Lipids were then extracted and the chloroform phase was adjusted to a 5-ml total volume, and triplicates of 50 ml in combination with standards were dried down by the addition of 10 ml of a 2:1 chloroform–Triton X-100 mixture. Triglyceride (TG) levels were then assayed using Infinity reagent (Thermo Fisher Scientific, Waltham, MA).

Systemic metabolic tests and blood chemistry. For the OGTTs, mice were fasted for 3 h prior to administration of glucose (2.5 g/kg of body weight) by gastric gavage. At various time points, venous tail blood samples were collected in heparin-coated capillary tubes. Glucose levels were measured using an oxidase-peroxidase assay (Sigma-Aldrich). Mice did not have access to food throughout the experiment. Serum TG levels (Infinity; Thermo Fisher Scientific) and free fatty acid (FFA) levels (NEFA-HR [2]); (Wako Pure Chemical Industries, Tokyo, Japan)& were assayed following a 3-h fast.

Protein analysis. Total protein was extracted by the methods described previously (10). The protein concentration was measured with a bicinchoninic acid (BCA) assay kit (Pierce). Proteins were then separated by 10% or 4 to 12% bis-Tris SDS gels (Invitrogen) and transferred to a polyvinylidene difluoride (PVDF) membrane (Millipore Corp., Temecula, CA). For immunoblotting, the primary antibodies for HIF1α (Novus) and adiponectin (45) were used, followed by secondary antibodies labeled with infrared dye emitting at 800 nm (Li-Cor Bioscience). The blots were analyzed with Odyssey software (version 2.1; Li-Cor Bioscience). Serum samples were also analyzed by immunoblotting with the method above. In addition, they were measured for levels of the following adipokines with enzyme-linked immunosorbent assay (ELISA) kits: adiponectin (Millipore), leptin (Millipore), and serum amyloid A3 (SAA3) (Millipore).

qPCR. Adipose and liver tissues were excised and quickly frozen in liquid nitrogen. Total RNAs were extracted from tissues in TRIzol (Invitrogen, Carlsbad, CA) using a TissueLyser (Qiagen, Valencia, CA) and then isolated using the RNeasy RNA extraction kit (Qiagen) by following the protocol from the company. The quality and quantity of the RNA were determined by absorbance at 260 and 280 nm. cDNAs were prepared by reverse transcribing 500 ng of total RNA with Superscript III reverse transcriptase and oligo(dT)$_{20}$ (Invitrogen). Quantitative real-time PCRs (qPCRs) were carried out on an ABI Prism 7900 HT sequence detection system (Applied Biosystems). The relative amounts of all mRNAs were calculated by using the comparative threshold cycle (C_T) method. The primer sequences have been published previously (10, 40). Hypoxanthine phosphoribosyltransferase (HPRT) or glyceraldehyde-3-phosphate dehydrogenase (GAPDH) mRNA was used as the invariant control.

Statistical analysis. All the results are presented as means ± standard deviations (SD). Differences between two groups were determined for statistical significance by a standard two-tailed Student *t* test. Differences between multiple groups were also determined by a one-way analysis of variance (ANOVA). Significance was accepted at a P value of <0.05.

RESULTS

Rapid adipose tissue expansion during HFD feeding is associated with low oxygen pressure in WAT. To determine the degree of hypoxia prevailing in a rapidly expanding mouse fat pad, we measured the oxygen pressure (pO_2) in the epididymal white adipose tissue (EWAT) during HFD feeding. To do so, we chose to use electron paramagnetic resonance (EPR) oximetry, which allows the direct measurement of absolute values of pO_2 with minimal invasion in intact white fat pads (41) (Fig. 1A). The yellow arrow in Fig. 1A indicates the oxygen probe, which has high *in vivo* sensitivity and specificity for pO_2 with nontoxic effects (42). During HFD feeding, the mice gained significant body weight (baseline, 29.5 ± 1.5 g, versus high-fat diet, 38.8 ± 1.5 g; $P < 0.001$) (Fig. 1B). This was accompanied by a worsening of the glucose tolerance (area under the curve [AUC] of glucose values, 33,360 ± 7,211 mg · min/dl versus 43,168 ± 7,306 mg · min/dl; $P = 0.009$) (data not shown). The increase in body weight was associated with a significant decrease in adipose tissue pO_2 (Fig. 1C) as measured by EPR oximetry (baseline, 27 ± 17 mm Hg, versus high-fat diet, 8 ± 10 mm Hg; $P = 0.017$). As a result, HIF1α was highly induced in EWAT (Fig. 1D). As a control, we also measured pO_2 in the gastrocnemius muscle. We found that there was no significant difference in pO_2. Notably, HIF1α induction in other tissues, such as brown adipose tissue (BAT) and the liver, is only marginal (Fig. 1E, top, and data not shown). The pO_2 measurements by EPR oximetry do not appear to induce or to be affected by fibrosis (Fig. 1A, bottom). Our data confirm the prevalence of hypoxic conditions in rapidly expanding fat tissues in HFD-fed mice.

The HIF1α inhibitor PX-478 selectively suppresses HIF1α and hence its target genes in WAT. PX-478 is a specific HIF1α inhibitor which effectively suppresses HIF1α in cancer cells at the levels of both mRNA and protein (26, 29, 30). To investigate the inhibitory efficacy in adipose tissue, we challenged 6-week-old mice with the HFD for 2 weeks. We then gavaged them daily with PX-478 in PBS at the dose of 5 mg/kg or with a vehicle only (PBS) for 3 days while continuing to feed them the HFD. Western blotting with anti-HIF1α antibodies indicated that PX-478 effectively suppressed HFD-mediated induction of HIF1α protein levels in EWAT (Fig. 1E). We also observed decreased HIF1α mRNA levels in EWAT of the treated mice (Fig. 1F). As a result, the direct HIF1α target genes induced by HFD feeding, such as the vascular endothelial growth factor A (VEGF-A), Glut1, leptin, and lysyl oxidase (LOX) genes, were downregulated upon PX-478 treatment (Fig. 1G). However, the nondirect target gene collagen III (Col3) was not affected by treatment in the acute phase (Fig. 1G). These observations in adipose tissue are consistent with findings in many cancer cell lines (29) and argue that PX-478 reaches effective concentrations in adipose tissue as well, leading to a reduction of HFD-induced HIF1α levels and hence its transcriptional target genes.

To rule out the potential toxic effects of PX-478, we measured the serum enzyme profiles reflecting myocardial or hepatocyte infarction. All the enzymes we measured, including aspartate transaminase (AST), lactate dehydrogenase (LDH) and creatine kinase (CK), did not show abnormal changes in PX-478-treated mice (see Fig. S2 in the supplemental material), suggesting that the dose of PX-478 that we used had no toxic effects.

Mice treated with PX-478 gain less body weight and exhibit resistance to an HFD challenge. We next investigated the impact of PX-478-mediated HIF1α suppression on metabolic parameters. The key question is whether the pharmacological inhibition of HIF1α has any impact on the gradual manifestation of metabolic dysfunction over the course of an HFD exposure. To address this question, we challenged 6-week-old mice with an HFD for 2 weeks. We then gavaged them with PX-478 in PBS at the dose of 5 mg/kg or with a vehicle only (PBS) for 7 weeks every second day, while continuing to expose them to the HFD. During the 7-week treatment regimen, PX-478-treated mice gained significantly less body weight than placebo-treated littermates (Fig. 2A). Notably, the differential body weight gain is apparent only in HFD-challenged groups. When mice are kept on a regular chow diet, no significant body weight differences can be observed (Fig. 2A). Chow feeding conditions are associated with minimal HIF1α induction in adipose tissue; hence, HIF1α activity is at a relatively low level (data not shown). The body weight difference on the HFD in the PX-478-treated mice is mainly due to a difference in fat mass (Fig. 2B). Moreover, the average size of adipocytes in PX-478-treated mice was also significantly smaller (Fig. 2C; quantification of the fat cell sizes is in Fig. 2D). This includes a reduced lipid accumulation in brown adipose tissue. An additional important control for the specific action of PX-478 is the fact that food intake was unaffected by HIF1α inhibition, since PX-478- and vehicle-treated mice consumed the same amount of food per gram of body weight throughout the treatment period (Fig. 2E). Collectively, these results in response to PX-478 treatment are in line with the reduced overall adiposity that these mice display.

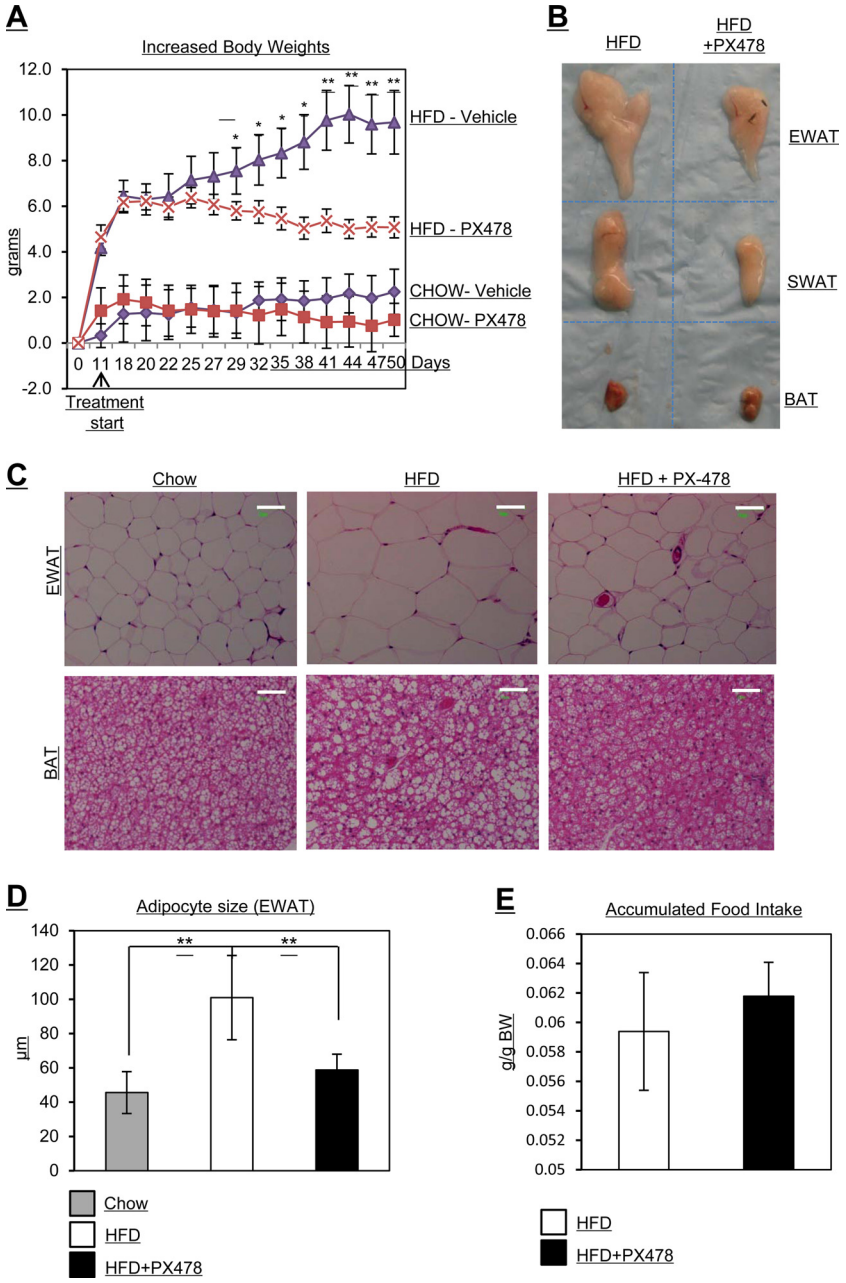

FIG 2 PX-478-treated mice gain less body weight, have smaller fat pads and smaller adipocytes, and exhibit reduced food intake under HFD challenge. (A) Body weight measurements in PX-478-treated and littermate control mice fed with regular chow (CHOW) or an HFD ($n = 5$ for each group). PX-478 treatment was started after HFD feeding for 11 days. *, $P < 0.05$; **, $P < 0.001$. (B) Comparison of sizes of different fat pads (EWAT, SWAT, and BAT) in PX-478-treated or control mice. (C) H&E staining of EWAT and BAT of mice fed regular chow, an HFD, and an HFD plus PX-478. The bars represent 50 μm. (D) Quantitative measurements of adipocyte sizes in EWAT of mice from the indicated groups. **, $P < 0.001$. (E) Accumulated food intake per day in PX-478-treated and littermate control mice ($n = 5$ for each group).

Mice treated with PX-478 exhibit improved glucose tolerance and increased energy expenditure. To investigate the metabolic consequences of PX-478 treatment, we performed OGTTs and also measured the fasting glucose levels. The OGTTs demonstrate that the response to an oral glucose challenge is significantly improved in PX-478-treated mice (Fig. 3A). The HFD-induced increase in fasting glucose levels was also normalized (Fig. 3B). Moreover, the ITTs demonstrate that PX-478-treated mice had improved insulin sensitivity (Fig. 3C). To further evaluate the metabolic benefits brought about by PX-478, we monitored the energy expenditure in metabolic chambers 2 weeks after initiation of PX-478 treatment. The oxygen consumption (VO_2) was significantly increased (Fig. 3D, upper left graph), reflecting an increase in energy expenditure in the PX-478-treated mice. PX-478-treated mice had no significant differences in the respiratory exchange rates (RER) (Fig. 3D, upper right graph). Surprisingly, the UCP-1 and PGC-1α genes were significantly upregulated in the subcutaneous WAT (SWAT) of PX-478-treated mice (Fig. 3E),

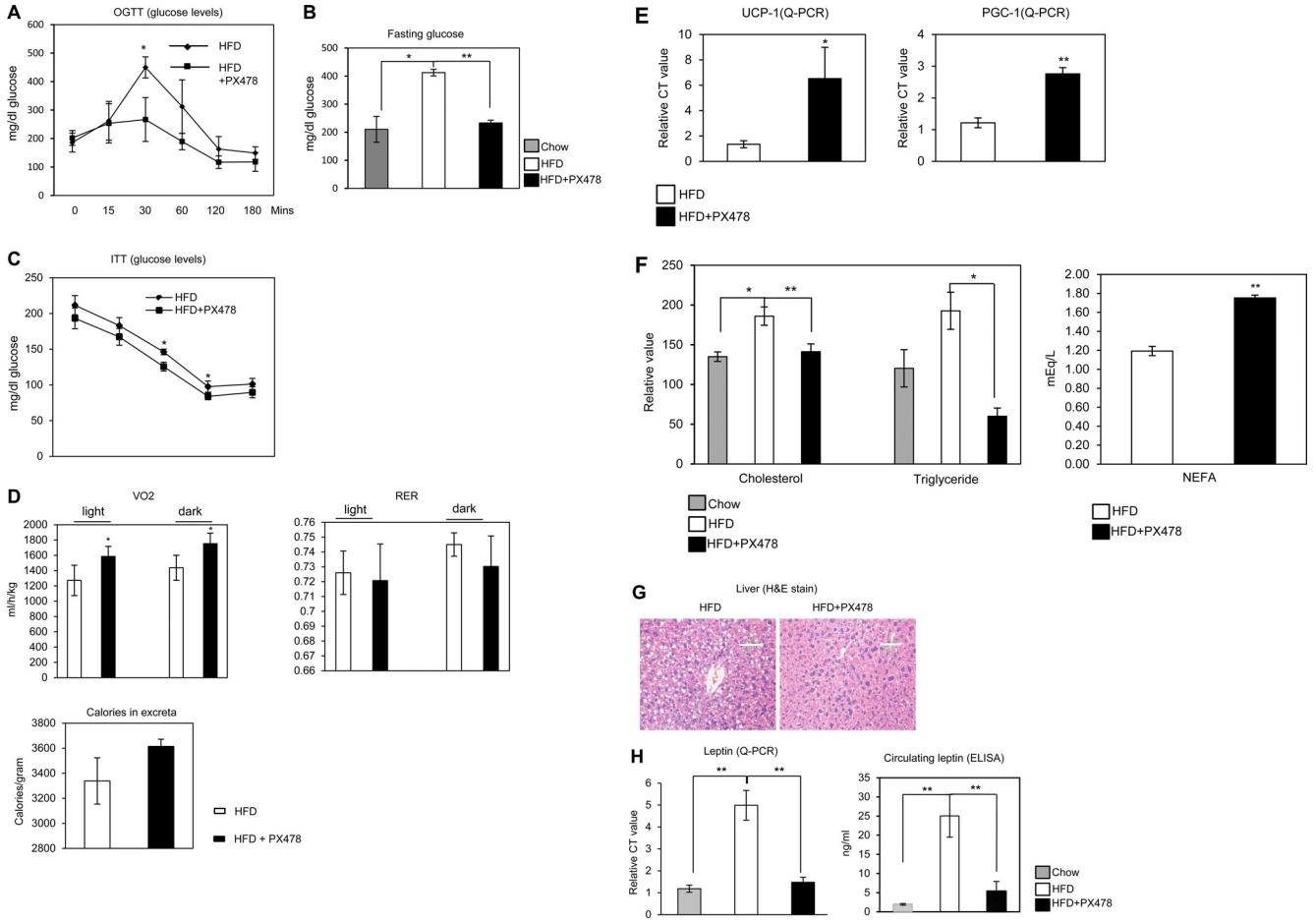

FIG 3 PX-478-treated mice exhibit improved glucose tolerance, increased energy expenditure, ameliorated circulating leptin levels, increased peripheral use of lipid, and hence decreased HFD-induced hepatic steatosis. (A) Circulating glucose levels measured during an OGTT in PX-478-treated or littermate control mice 6 weeks after HFD feeding ($n = 5$ for each group). The difference at each time point was determined by a Student t test. *, $P < 0.05$. (B) Circulating glucose levels in mice fed chow, an HFD, and an HFD plus PX-478 12 h after fasting. *, $P < 0.05$; **, $P < 0.001$ ($n = 5$ for each group). (C) Circulating glucose levels measured during an ITT in PX-478-treated mice or the littermate controls 2 weeks after PX-478 treatment. (D) Indirect calorimetry was performed in a TSE system by housing PX-478-treated mice or littermate controls after PX-478 treatment for 2 weeks. The mice were acclimated for 1 week in the metabolic chambers before the measurements were started. VO_2 and RER (VCO_2/VO_2) were analyzed in light (day) or dark (night) cycles. *, $P < 0.05$. The total calories in excreta were measured by collecting the stools from each cage for 3 days. (E) Serum cholesterol, triglyceride, and NEFA levels in mice fed chow, an HFD, and an HFD plus PX-478 ($n = 5$ for each group) after fasting for 12 h. *, $P < 0.05$; **, $P < 0.001$. (F) qPCR analysis for UCP-1 and PGC-1 in mice fed an HFD and an HFD plus PX-478 ($n = 5$ for each group). *, $P < 0.05$; **, $P < 0.001$. (G) H&E staining of the liver tissues from mice fed an HFD and an HFD plus PX-478. The bars represent 100 μm. (H) Leptin mRNA levels in EWAT (left) and circulating leptin (right) levels in mice fed chow, an HFD, and an HFD plus PX-478 ($n = 5$ for each group). **, $P < 0.001$.

further highlighting the potential for enhanced energy expenditure in these mice. Collectively, PX-478 treatment therefore leads to improved glucose tolerance and increased energy expenditure. Though the levels of food intake were comparable (Fig. 2E), the increased caloric content in the excreta collected from PX-478-treated mice (Fig. 3D, bottom graph) combined with the increase in overall energy expenditure offers at least a partial explanation for the differential weight gain of the PX-478-treated group on the high-fat diet.

PX-478 treatment promotes an increase in lipid clearance, a decrease in HFD-induced hepatic steatosis, and normalization of circulating leptin levels caused by HFD feeding. To determine whether PX-478 treatment also improves lipid metabolism, we assessed plasma lipid parameters. The HFD-induced elevated levels of plasma cholesterol and triglycerides were normalized in the PX-478-treated mice (Fig. 3F). Furthermore, the degree of HFD-induced hepatic steatosis was significantly reduced (Fig. 3G), suggesting that HIF1α inhibition is also associated with improvements in lipid metabolism. Surprisingly, the circulating nonesterified free fatty acid levels (NEFAs) increased in PX-478-treated mice (Fig. 3F, right graph), suggesting enhanced lipolysis in the fat tissues of treated mice. Leptin levels in adipocytes have been suspected to be at least in part governed by local HIF1α activity *in vitro* and are abnormally high under local hypoxic conditions in adipose tissue (46). As a result, exposure to HFD also augments leptin production and release (47). Indeed, we observed higher expression of leptin in HFD-fed mice (Fig. 3H, left graph). PX-478 treatment nearly normalized the abnormally high leptin expression induced by the HFD. In line with these changes, we observed higher levels of circulating leptin in HFD-fed mice (Fig. 3H, right graph), and PX-478 treatment normalized the abnormally high leptin pro-

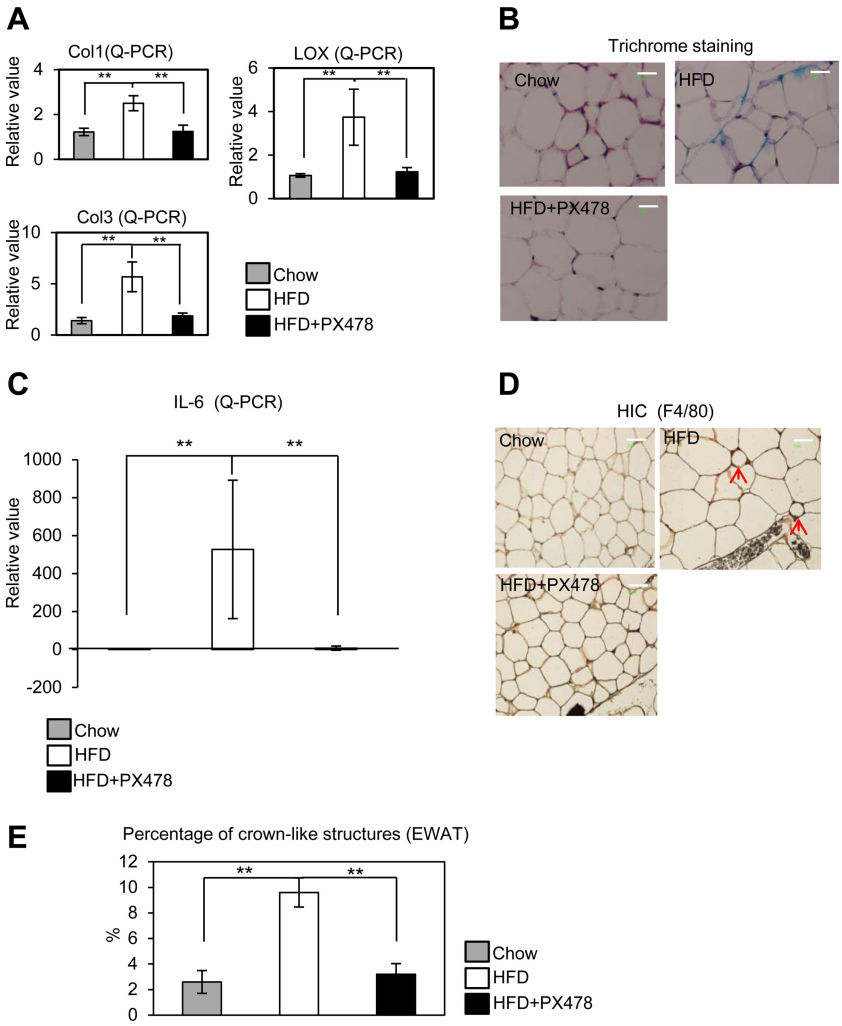

FIG 4 PX-478 treatment suppresses fibrosis and inflammation in EWAT induced by an HFD. (A) qPCR analysis for collagens (I and III) and their fiber linker enzyme LOX in mice fed chow, an HFD, and an HFD plus PX-478 ($n = 5$ for each group). **, $P < 0.001$. (B) Masson's trichrome staining in EWAT of mice fed chow, an HFD, and an HFD plus PX-478. (C) qPCR for IL-6 in EWAT of mice fed chow, an HFD, and an HFD plus PX-478 ($n = 5$ for each group). **, $P < 0.001$. (D) Immunohistochemical staining of F4/80 in EWAT in mice fed chow, an HFD, and an HFD plus PX-478. The arrows indicate the crown-like structures formed by macrophage aggregation in HFD-fed mice. (E) Quantitative measurements of the numbers of crown-like structures in mice fed chow, an HFD, and an HFD plus PX-478 ($n = 5$ for each group). **, $P < 0.001$. Bars, 50 μm.

tein levels induced by the HFD. While this may in part be due to the reduction of overall weight gain during HFD exposure, it also relates directly to the lack of HIF1α-mediated transcriptional activation caused by PX-478. To our surprise, adiponectin expression and the circulating levels were only slightly increased in the PX-478-treated mice and are therefore unlikely to be key mediators of the metabolic improvements (see Fig. S3 in the supplemental material).

PX-478 treatment suppresses fibrosis and reduces local inflammation in WAT during HFD exposure. We have previously demonstrated that a gain-of-function mutant of HIF1α in adipose tissue leads to a pathological setting and triggers a local fibrotic response (10). In this study, we sought to determine whether these pathological changes conventionally associated with a HFD challenge can be suppressed by specific HIF1α inhibition. Consistent with the significant decrease observed in the levels of HIF1α in the PX-478-treated group (Fig. 1E), the fibrotic collagens I and III (Col1 and Col3) were also significantly downregulated (Fig. 4A). Importantly, LOX, a direct HIF1α target involved in the cross-linking of collagen fibers in adipose tissue (10), was downregulated in PX-478-treated mice (Fig. 4A). In line with these transcriptional changes, Masson's trichrome stain of SWAT indicates that the extracellular matrix (ECM) accumulation is significantly reduced in the PX-478-treated mice (Fig. 4B).

Previously, we and others demonstrated that fibrosis induced by HIF1α is an initial step toward increased adipocyte necrosis, which eventually leads to increased macrophage accumulation and inflammation in the dysfunctional fat tissue (10, 48). We determined whether HIF1α inhibition by PX-478 suppresses the inflammatory response generally induced by HFD. Indeed, the local mRNA levels of interleukin 6 (IL-6) were significantly upregulated by HFD and were suppressed by PX-478 treatment (Fig. 4C). Immunohistochemical analysis of EWAT with antibodies against the macrophage marker F4/80 further confirms a reduced frequency of crown-like structures (CLS) surrounding dysfunctional and dead fat cells in the PX-478-treated mice (Fig. 4D and E). Local

inhibition of HIF1α by PX-478 in adipose tissue therefore not only suppresses pathological accumulation of ECM components but also, secondary to that, reduces local inflammation indirectly.

The HIF1α inhibitor digoxin suppresses HIF1α target genes in WAT and improves insulin sensitivity of the treated mice. To confirm the effects of HIF1α inhibition *in vivo* by PX-478, we tested the inhibitory efficacy of another HIF1α inhibitor, digoxin, in adipose tissue further. We challenged 6-week-old mice with an HFD for 2 weeks. We then injected (i.p.) them with digoxin in PBS at the dose of 2 mg/kg or with a vehicle only (PBS) for 14 days while continuing to feed them the HFD. We observed a trend of decreased HIF1α mRNA levels in EWAT of the treated mice (see Fig. S4A in the supplemental material). As a result of the inhibition, the direct HIF1α target genes induced by HFD feeding, such as the VEGF-A, Glut1, leptin, and LOX genes, were significantly downregulated upon digoxin treatment (see Fig. S4A). These observations in adipose tissue are consistent with the findings with the PX-478 treatment.

We performed an OGTT and an ITT 12 days after digoxin treatment. The results indicate that the digoxin-treated mice had an improved glucose tolerance and were more insulin sensitive (see Fig. S4B in the supplemental material). Collectively, the digoxin treatment yielded results similar to those with the PX-478 administration.

Generation of transgenic mice with adipose tissue-specific overexpression of dn-HIF1α. Pharmacological inhibition with PX-478 affects HIF1α system-wide. Even though in the context of excess nutrient intake, HIF1α is relatively selectively induced in adipose tissue, we wanted to find out how much of the PX-478 effect is due to HIF1α inhibition specifically in adipocytes. We therefore sought to genetically confirm these results by manipulating HIF1α in an adipocyte-specific way. We established a double transgenic mouse strain employing a tetracycline-inducible system. Figure 5A shows a schematic representation of the mouse model. We have previously described our adipocyte-specific tetracycline response element-driven (TRE) system (40). In this model, this TRE promoter is regulated by the reverse tetracycline-dependent transcriptional activator (rtTA), whose expression is under the control of the adipose tissue-specific adiponectin promoter (39). In this case, we used the system to drive expression of dn-HIF1α in the adipocyte that we can induce in the presence of doxycycline. To effectively inhibit endogenous HIF1α, we used double transgenic mice, i.e., homozygous versions for both Adn-rtTA and TRE-dn-HIF1α transgenes. Three days after normal chow plus treatment with 600 mg/kg of DOX, the dn-HIF1α mRNA levels were highly induced in different adipose tissues, especially in EWAT and SWAT (Fig. 5B), while no induction was observed in other tissues (see Fig. S5 in the supplemental material). As a result, direct target genes of HIF1α, such as the VEGF-A, Glut1, leptin, and LOX genes, were all significantly downregulated in EWAT of the dn-HIF1α transgenic mice (Fig. 5C).

Overexpression of dn-HIF1α in adipose tissue decreases body weight gain and adipocyte size and improves insulin sensitivity in HFD-challenged mice. To investigate the metabolic consequences of HIF1α blockage induced by genetic means, dn-HIF1α mice and wild-type littermate controls were challenged with an HFD plus 600 mg/kg of DOX for 8 weeks. During the 8-week HFD exposure, dn-HIF1α mice gained less weight (Fig. 6A) and exhibited improved glucose tolerance and insulin sensitivity as judged by an oral glucose tolerance test and an insulin tolerance test (Fig. 6B). Histological examination of H&E-stained slides indicated that the size of fat cells in both WAT and BAT were much smaller in dn-HIF1α mice (Fig. 6C; quantification in graph). Collectively, genetic disruption of HIF1α function by overexpression of dn-HIF1α specifically in adipocytes brings about metabolic improvements qualitatively consistent with the results obtained with system-wide pharmacological inhibition with PX-478, despite the fact that we did not reach the same extent of inhibition genetically as in the context of the pharmacological PX-478 inhibitor treatment.

Overexpression of dn-HIF1α in AT leads to an increase in energy expenditure. We performed additional experiments paralleling the assays performed for the pharmacological inhibition. We monitored the energy expenditure in the dn-HIF1α transgenic mice and their littermate controls in metabolic chambers. The VO_2 was significantly increased (Fig. 6D, upper left graph), while the RER and food intake displayed no changes (Fig. 6D, upper right and bottom left graphs), reflecting an increase in energy expenditure in dn-HIF1α transgenic mice. Surprisingly, the caloric content of the excreta generated by the transgenic mice was higher (Fig. 6D, bottom right graph). Together with the comparable food intake, these observations at least partially explain the reduced body weight gain in the transgenic mice on the high fat diet.

Overexpression of dn-HIF1α promotes an increase in lipid clearance, a decrease in HFD-induced hepatic steatosis, and normalization of circulating leptin levels caused by HFD feeding. To determine whether the dn-HIF1α overexpression in AT also improves lipid metabolism, we measured plasma triglyceride and NEFA levels. Both triglyceride and NEFA levels were significantly lower in dn-HIF1α transgenic mice (Fig. 7A). Liver histology also shows a clear-cut reduction in steatosis in the transgenic mice (Fig. 7B). Since the circulating leptin levels were very sensitive to pharmacological inhibition of HIF1α by PX-478 (Fig. 3F), we wanted to test leptin levels in the genetic model as well. Indeed, we also observed a dramatic decrease of both leptin expression and circulating leptin in dn-HIF1α mice (Fig. 7C). This further demonstrates the importance of the HIF1α contribution toward leptin expression *in vivo*. Even though adiponectin expression was significantly upregulated in the adipose tissue of dn-HIF1α transgenic mice, the circulating adiponectin levels were only slightly increased (see Fig. S6A and B in the supplemental material; quantitative measurements of the band densities are shown in Fig. S6C). Overexpression of dn-HIF1α therefore displays, to a large extent, the same phenotype as the use of the PX-478 inhibitor, albeit in a somewhat more attenuated fashion.

Overexpression of dn-HIF1α suppresses fibrosis and reduces local inflammation in WAT during HFD exposure. To further confirm the beneficial effects of disruption of HIF1α by dn-HIF1α overexpression in obese mice, we sought to determine whether dn-HIF1α can suppress the fibrosis and pathological ECM expansion during HFD exposure. qPCR shows that the endogenous HIF1α and a direct HIF1α transcriptional target, LOX, were also reduced (Fig. 8A; see also Fig. S7A in the supplemental material). As a result, the fibrotic collagens I, II, and VI (Col1, Col3, and Col6) were significantly reduced in EWAT of dn-HIF1α mice (Fig. 8A). Consistent with the gene expression analysis, histological examination of SWAT with Masson's trichrome stain shows that the extracellular matrix accumulation is significantly decreased in the transgenic mice (Fig. 8B). In line with that, we further determined whether dn-HIF1α expression also causes a

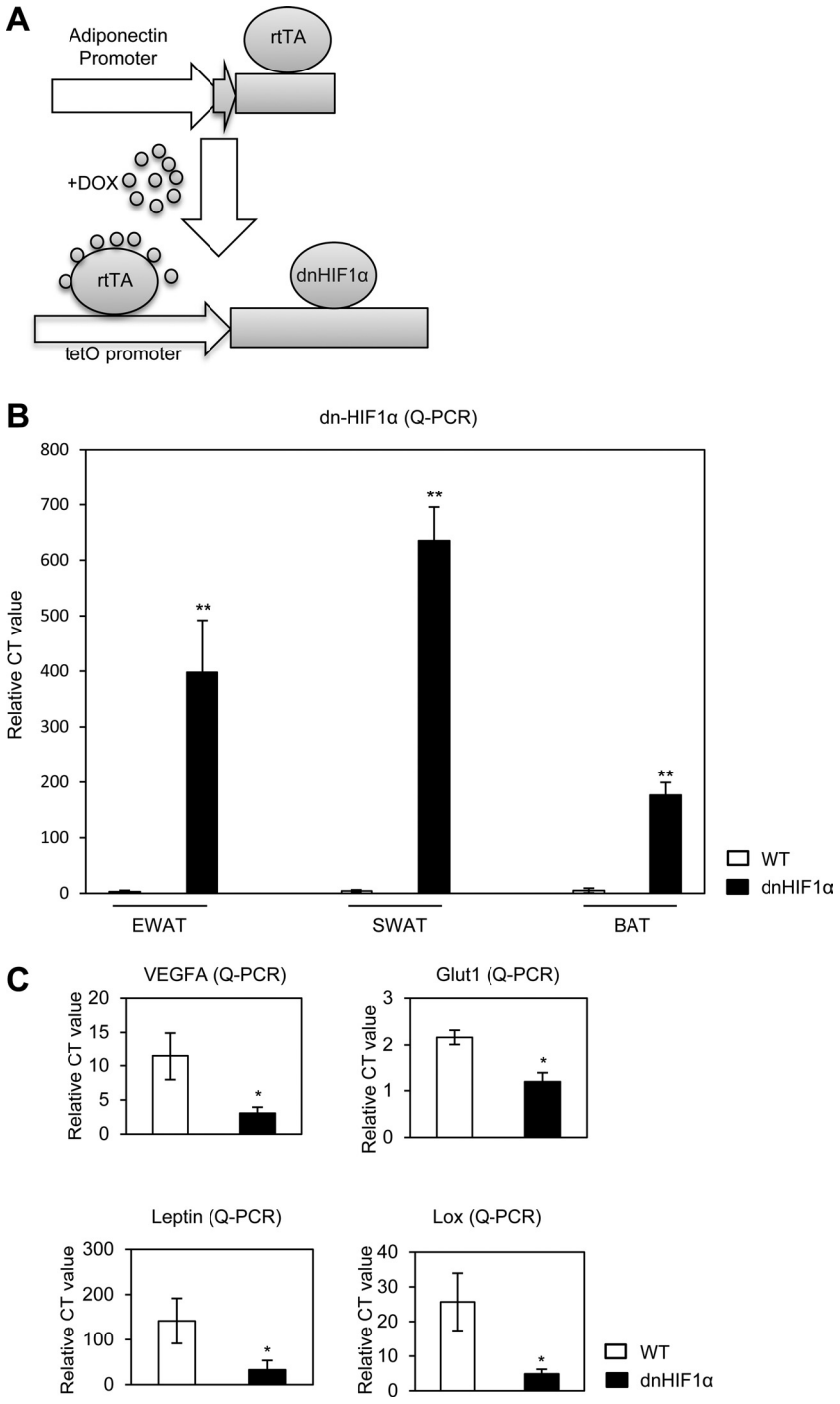

FIG 5 dn-HIF1α induction exclusively in adipose tissue blocks its direct target genes in WAT. (A) Schematic representative of a mouse model for DOX-inducible adipose tissue-specific overexpression of dn-HIF1α. (B) qPCR analysis of dn-HIF1α overexpression in different fat pads (EWAT, SWAT, and BAT) in the double transgenic mice and their littermate controls 3 days after treatment with chow plus DOX. (C) qPCR analysis of direct HIF1α target genes in EWAT of the double transgenic mice and their littermate controls 3 days after treatment with chow plus DOX.

suppression of inflammation caused by the HFD. Indeed, we found that mRNA levels of both the macrophage marker F4/80 and the acute-phase inflammation marker serum amyloid A3 (SAA3) were significantly suppressed in dn-HIF1α mice (Fig. 8C, upper graphs). In line with the gene expression, circulating SAA protein levels were dramatically decreased in dn-HIF1α mice as well (Fig. 8C, bottom graph), reflecting a reduced inflammatory response to the HFD in fat pads of transgenic mice.

DISCUSSION

Hypoxia has been linked to the pathological changes associated with obesity (4–6, 10). HIF1α is an essential mediator of the anti-

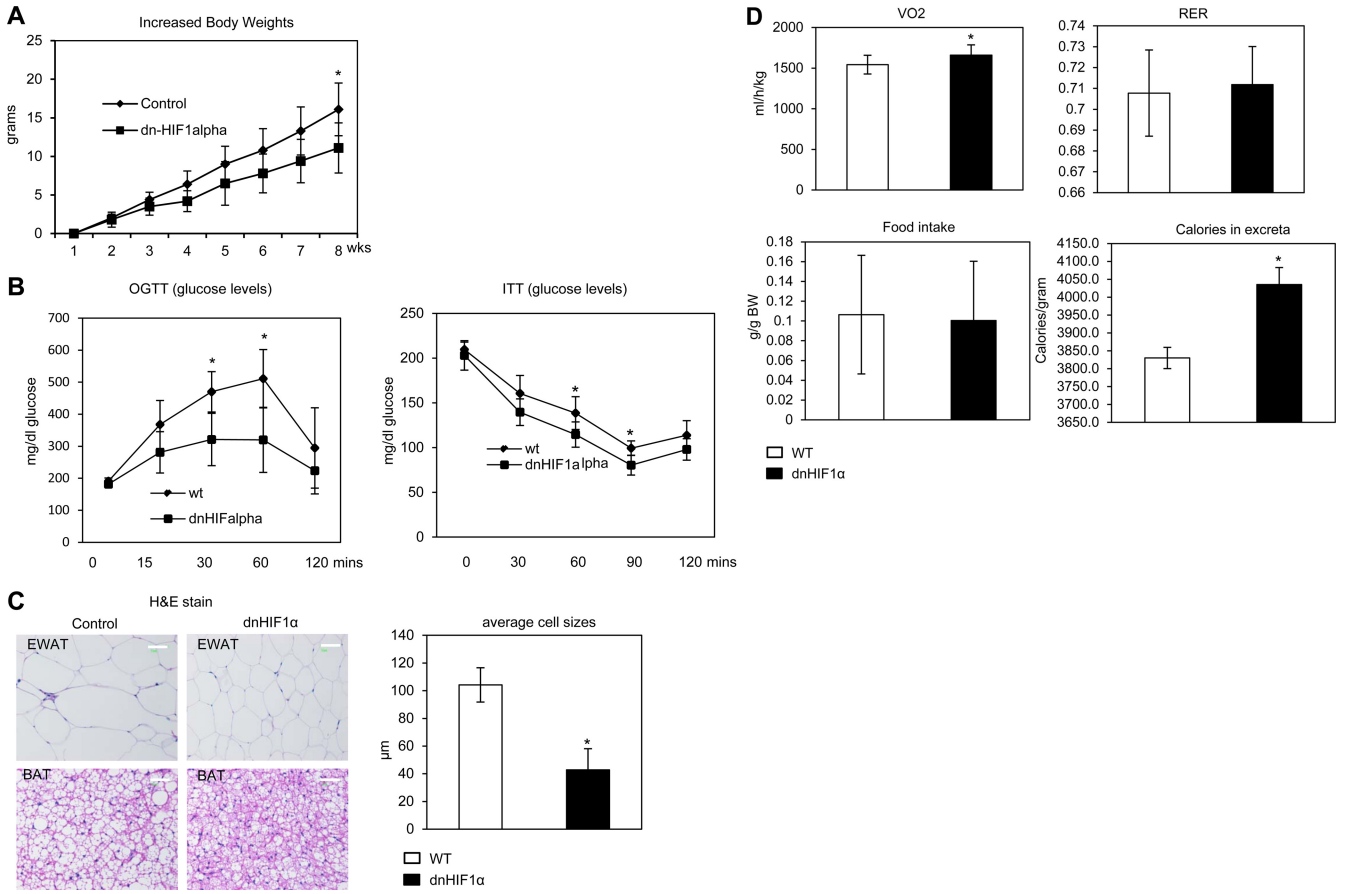

FIG 6 Overexpression of dn-HIF1α locally in adipose tissue ameliorates development of obesity, increases energy expenditure, and improves lipid metabolism under an HFD challenge. (A) Body weight gain in dn-HIF1α and their littermate controls during treatment with an HFD plus 600 mg/kg of DOX for 8 weeks ($n = 5$ for each groups). *, $P < 0.05$. (B) Circulating glucose levels during an OGTT and an ITT in dn-HIF1α and their littermate controls after treatment with an HFD plus DOX for 5 weeks ($n = 5$ for each group). *, $P < 0.05$. (C) H&E staining for EWAT and BAT of dn-HIF1α mice and their littermate controls 8 weeks after treatment with an HFD plus DOX. The bars represent 50 μm (left). The graph on the right shows quantification of the fat cells in EWAT in control and dnHIF1 transgenic groups. (D) Indirect calorimetry was performed in a TSE system for dn-HIF1α transgenic mice and their littermate controls after feeding with an HFD plus DOX for 6 weeks. VO_2, RER (VCO_2/VO_2), and core body heat were analyzed as the average results during a 24-h light-dark cycle since there are no differences between the light and dark cycles ($n = 5$ for each group). *, $P < 0.05$.

hypoxic response under hypoxic stress in many cell types. It is also induced over the course of progression toward an obese fat pad. As one of the earliest events during adipose tissue expansion, HIF1α induction presents a critical step in the sequential process of obesity-associated adipose tissue dysfunction (10). Intriguingly, unlike its action in most other tissues, including tumor tissues, HIF1α stabilization in adipose tissue does not lead to the induction of proangiogenic factors, such as VEGF (7, 10). Therefore, hypoxic fat pads are very ineffective at mounting a proangiogenic response. Even though quantitatively less prominent, this is also true in obese human adipose tissue (7). On the other hand, an alternative HIF1α-mediated transcriptional program is significantly induced, mainly leading to an enhanced fibrotic response. The transcription of many extracellular matrix constituents (ECM) ultimately leads to an inflexible "shell" around individual adipocytes, which results in an increased rate of adipocyte necrosis, ultimately triggering an increased rate of macrophage infiltration and inflammation (10, 20). In this study, we used an *in vivo* oxygen sensor probe in an HFD-fed obese model and not only demonstrated low oxygen pressure in rapidly expanding WAT but also confirmed that HIF1α is induced under these conditions. A number of recent studies implicate HIF1α in the pathophysiology of obesity (49, 50). This prevailing obesity-associated hypoxia (and concomitant HIF1α induction) is mainly observed in white fat pads, while the induction in other tissues, such as brown adipose tissue (BAT) and liver, is only marginal. This highlights that adipose tissue is uniquely affected under these conditions and suggests the possibility that systemic HIF1α inhibition may primarily exert its therapeutic effects through action in adipose tissue. The data presented establish this phenomenon for the first time.

Furthermore, given the central role of HIF1α in the activation of numerous pathways responsible for metabolic dysfunction demonstrated in gain-of-function studies (10), we wanted to test whether the inactivation of HIF1α action specifically targeted to adipocytes is a reasonable therapeutic strategy for obesity-associated metabolic dysfunction. Surprisingly, there are no reports in the literature that focus on targeted therapies in this area despite widespread efforts in the context of cancer (21, 22, 51). We therefore investigated the effects of one of the more promising HIF1α inhibitors, PX-478, on obesity-related metabolic dysfunction. PX-

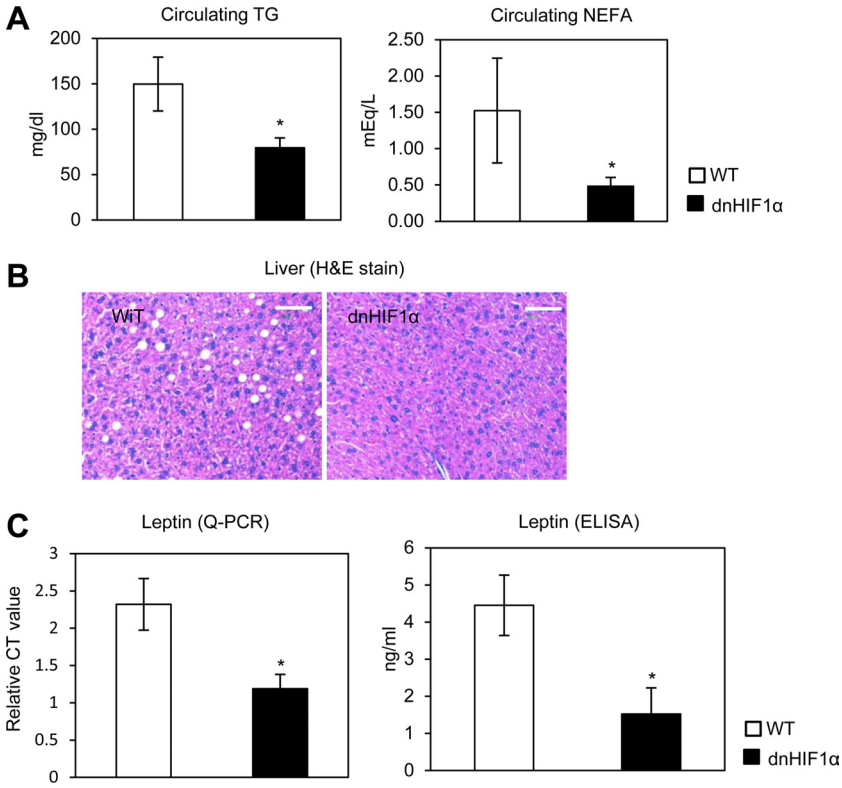

FIG 7 Overexpression of dn-HIF1α locally in adipose tissue increases peripheral use of lipid, decreases HFD-induced hepatic steatosis, and regulates circulating leptin levels. (A) Liver triglyceride (left) and cholesterol (right) in dn-HIF1α transgenic mice and their littermate controls after treatment with an HFD plus DOX for 8 weeks ($n = 5$ for each group). *, $P < 0.05$. (B) H&E staining for liver tissues in dn-HIF1α transgenic mice and their littermate controls. The bars represent 50 μm. (C) qPCR analysis of leptin in EWAT (left) and circulating leptin levels measured by ELISA (right) in dn-HIF1α transgenic mice and their littermate control mice after treatment with an HFD plus DOX for 8 weeks ($n = 5$ for each group). *, $P < 0.05$.

478 has been well characterized both in cancer cell lines and in cancer mouse models (26–33, 52). The main impact of PX-478 in different tumor models is to downregulate Glut1 levels (29, 30), suggesting that the thrust of its antimitogenic activity is mediated through its regulation of glucose metabolism. Consistent with this model, PX-478 has very limited effects on tumor angiogenesis (21).

PX-478 is orally available (29). We therefore treated the mice with PX-478 by gastric gavage. During the 5 weeks of treatment, we observed a lower rate of weight gain compared to placebo treatment, mainly due to differences in fat mass in PX-478-treated mice. PX-478 treatment also exhibited improved glucose tolerance. In addition, circulating glucose and triglyceride levels were decreased in the PX-478-treated mice. These metabolic improvements are likely due to the reduced overall adiposity in these mice, which is reflected by the smaller adipocyte size, the reduced fat pads, and the altered circulating adipokine levels. Therefore, we expect these PX-478-treated mice to display a full metabolic improvement across the board, and all parameters tested suggest that this is indeed the case. Our metabolic studies also show that PX-478-treated mice display an increased basal metabolic rate and energy expenditure, without any changes observed with respect to food intake. Furthermore, the "browning" markers UCP-1 and PGC-1α were significantly upregulated in SWATs of PX-478-treated mice, suggesting a browning program in these mice. We do not know what the underlying mechanistic basis is for the increased energy expenditure upon HIF1α inhibition. Since this is a phenomenon seen both with systemic pharmacological inhibition and with adipocyte-specific manipulation of the pathway, it suggests that an adipocyte-derived signal is responsible for this phenomenon. Leptin would be an excellent candidate as a mediator of these effects. Leptin is a critical adipokine that regulates energy homeostasis through the regulation of food intake and energy expenditure (53). However, circulating leptin levels are decreased upon HIF1α inhibition, making it an unlikely effector. As a direct target of HIF1α, leptin levels were dramatically decreased in both mouse models, yet food intake was normal. This suggests that these models are more leptin sensitive under this HFD insult. We were surprised to see that the manipulation of HIF1α levels had such a profound impact on leptin expression and release. Previously, Wang et al. reported that leptin is expressed only in well-differentiated adipocytes under normoxic conditions (46). However, under hypoxic conditions, preadipocytes express and secrete leptin as well (46). Our data suggest that the unique secretion pattern in preadipocytes is regulated by HIF1α and that the effect can be inhibited by PX-478 treatment or overexpression of a dn-HIF1α. Indeed, Ambrosini and colleagues suggest that the leptin gene is a direct target for HIF1α. These authors have identified a hypoxia response element (HRE) in the leptin promoter (64). Our studies highlight the importance of these findings in the *in vivo* setting. Leptin levels in circulation are generally directly proportional to fat mass. An unresolved issue is how an individual fat cell

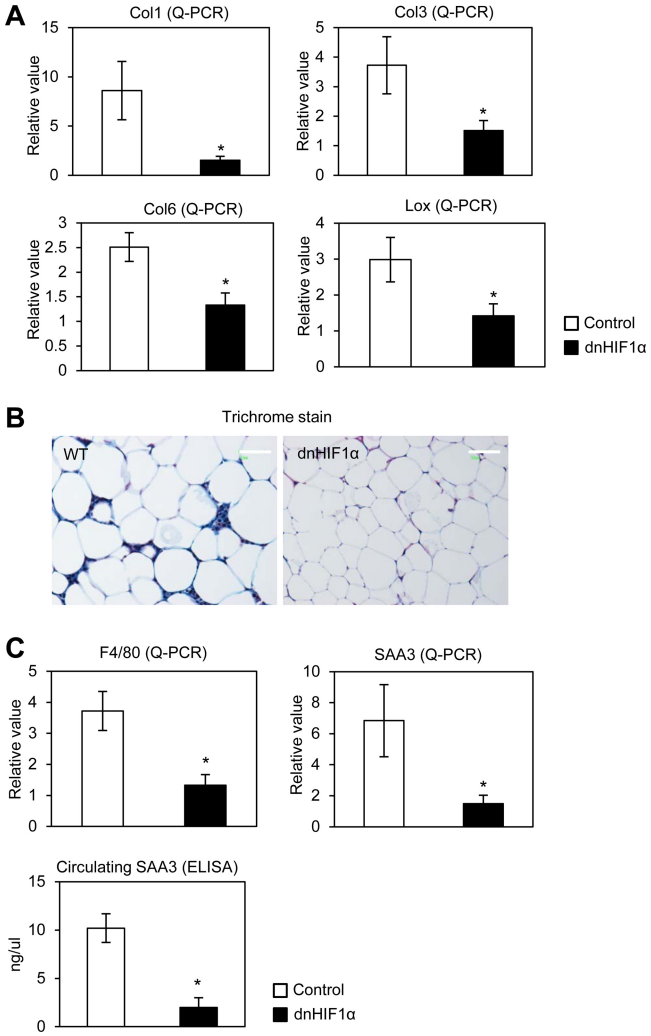

FIG 8 Overexpression of dn-HIF1α locally in adipose tissue suppresses fibrosis and inflammation induced by an HFD. (A) qPCR analysis for collagens (I, II, and VI) and LOX in dn-HIF1α transgenic mice and their littermate controls ($n = 5$ for each group). *, $P < 0.05$. (B) Masson's trichrome stain for EWAT of dn-HIF1α transgenic mice (left) and their littermate controls (right). The bars indicate 100 μm. (C) qPCR analysis for F4/80 and SAA3 for EWAT in dn-HIF1α transgenic mice and their littermate controls ($n = 5$ for each group, upper graphs) and circulating SAA3 levels in dn-HIF1α mice and their littermate controls ($n = 5$ for each group, lower graph). *, $P < 0.05$.

gauges its own size and consequently adjusts its leptin expression levels. A HIF1α-mediated mechanism would be an excellent mediator of these effects. Large cells are chronically hypoxic and hence will enjoy higher HIF1α levels, leading to increased leptin transcription and release. Therefore, we can manipulate leptin levels very effectively *in vivo* by manipulating HIF1α activity, independent of fat mass. To our surprise, we did not observe significant changes in circulating adiponectin levels by either HIF1α inhibition paradigm employed. However, the dramatic decrease in leptin levels, together with downregulation of other adipokines, such as IL-6, suggests decreased adiposity in these models.

Fibrosis in adipose tissue plays critical roles in downstream events, which lead to further metabolic dysfunction in fat pads (20). Reduced adipose tissue fibrosis can be achieved through a genetic disruption of collagen VI. This results in an overall improved metabolic phenotype (20). Since we previously found that hypoxia-induced HIF1α in adipose tissue mainly upregulates fibrillar collagens and the enzyme LOX (which plays an important role in collagen fiber formation [10]), we focused on the regulation of these HIF1α target genes by HIF1α inhibition. As expected, collagens I and III and the collagen cross-linking LOX enzyme induced by HFD feeding were dramatically downregulated by PX-478 and dn-HIF1α. Trichrome staining further confirms that a local state of fibrosis induced by HFD was suppressed by HIF1α inhibition.

The development of inflammation in adipose tissue has been linked to many other metabolic syndromes (55, 56). During fat pad expansion, monocytes and macrophages infiltrate into adipose tissue (57, 58). The local state of fibrosis caused by HIF1α within adipose tissue can be the initiating factor for monocyte and macrophage infiltration and inflammation, even though it is not firmly established what the key signal is for this process (10). We observed significantly decreased expression of inflammatory factors such as IL-6 by qPCR in EWAT. Along with these transcriptional changes, a reduced frequency of crown-like structures surrounding adipocytes in the PX-478-treated group could be seen.

We repeated the studies performed with the pharmacological inhibitor with a local overexpression of a dn-HIF1α protein. The dn-HIF1α protein is a fragment of wild-type HIF1α lacking the DNA-binding domain, the transactivation domain, and the oxygen-dependent domain (ODD) (34, 35). This mutant has been demonstrated to effectively reduce HIF1α activity in neurons and pancreatic cancer cells. In our system, we took advantage of the inducible and tissue-specific nature of our construct. We initiated the adipose tissue-specific overexpression only upon endogenous HIF1α induction with the HFD challenge. In that way, we selectively blocked the function of endogenous HIF1α only upon HFD induction. By using this model, we were able to observe metabolically beneficial outcomes similar to those with PX-478 treatment. We did not achieve in all instances quantitatively the same effects as with the pharmacological inhibitor, even though qualitatively, we obtained the same results across the board. This is likely due to the lack of a complete inhibition of endogenous HIF1α activity using a dominant negative version of HIF1α. Complete inhibition can be achieved more effectively using pharmacological agents, such as PX-478.

Although we confirmed all the metabolic effects obtained pharmacologically with PX-478 with an adipose tissue-specific dn-HIF1α overexpression model, we noticed that the magnitude of the effects in the transgenic mouse model were milder than in the PX-478-treated mice. This suggests that in addition to the local effects in adipose tissue, PX-478 may also suppress HIF1α functions in other tissues. Of note, as an active metabolic site, skeletal muscle experiences dramatic oxygen level fluctuations during endurance exercise. As a result, hypoxic conditions may develop in that setting, and HIF1α-mediated pathways play an important metabolic role (54, 59, 60). Moreover, HIF1α has also been shown to play a role in liver metabolism by regulating hepatic glucose homeostasis (61). Even though neither of these organs displays hypoxia under conditions of HFD exposure, we cannot exclude the possibility that PX-478-mediated effects in muscle and liver contribute to the metabolic improvements observed.

In conclusion, our findings in combination with reports from others (10, 49, 50) suggest that HIF1α, a factor induced early in adipose tissue during the development of obesity and critically

involved in the pathogenesis of insulin resistance in adipose tissue, is an attractive drug target. However, even though several recent reports confirmed that adipose tissue in humans is also poorly oxygenated in the obese (62, 63), we do not know whether these hypoxic conditions are sufficient to induce high levels of HIF1α. Human adipose tissue expansion in most instances occurs over much more prolonged periods, allowing even modest proangiogenic activity to at least partially vascularize expanding pads. Nevertheless, many common features between rodent and human adipose tissue expansion are shared, and the basic lessons learned from the studies here warrant further investigation in a clinical setting as well.

ACKNOWLEDGMENTS

We thank Oncothyreon Inc. for providing the PX-478 compound, members in the Scherer laboratory for insightful discussion and technical assistance, John Shelton and James Richardson in the Pathology Core at UT Southwestern for helpful advice with histology, the Transgenic Core Facility at UT Southwestern under the direction of Bob Hammer for generating adiponectin-rtTA and TRE-dn-HIF1α transgenic mice, and the Metabolic Core at UT Southwestern for phenotyping efforts. We also thank P. Kuppusamy at The Ohio State University for generously providing the LiNc-BuO EPR probes.

This work was supported by NIH grants R01-DK55758, RC1DK086629, and P01DK088761 (to P.E.S.) and NIH grant HL093463 and Tzagournis Medical Research Endowment Funds of The Ohio State University (to U.J.M.).

We declare that we have no conflict of interest.

REFERENCES

1. **Sun K, Kusminski CM, Scherer PE.** 2011. Adipose tissue remodeling and obesity. J. Clin. Invest. **121**:2094–2101.
2. **Arner E, Westermark PO, Spalding KL, Britton T, Ryden M, Frisen J, Bernard S, Arner P.** 2010. Adipocyte turnover: relevance to human adipose tissue morphology. Diabetes **59**:105–109.
3. **Weyer C, Foley JE, Bogardus C, Tataranni PA, Pratley RE.** 2000. Enlarged subcutaneous abdominal adipocyte size, but not obesity itself, predicts type II diabetes independent of insulin resistance. Diabetologia **43**:1498–1506.
4. **Hosogai N, Fukuhara A, Oshima K, Miyata Y, Tanaka S, Segawa K, Furukawa S, Tochino Y, Komuro R, Matsuda M, Shimomura I.** 2007. Adipose tissue hypoxia in obesity and its impact on adipocytokine dysregulation. Diabetes **56**:901–911.
5. **Ye J.** 2009. Emerging role of adipose tissue hypoxia in obesity and insulin resistance. Int. J. Obes. (Lond.) **33**:54–66.
6. **Yin J, Gao Z, He Q, Zhou D, Guo Z, Ye J.** 2009. Role of hypoxia in obesity-induced disorders of glucose and lipid metabolism in adipose tissue. Am. J. Physiol. Endocrinol. Metab. **296**:E333–E342.
7. **Pasarica M, Sereda OR, Redman LM, Albarado DC, Hymel DT, Roan LE, Rood JC, Burk DH, Smith SR.** 2009. Reduced adipose tissue oxygenation in human obesity: evidence for rarefaction, macrophage chemotaxis, and inflammation without an angiogenic response. Diabetes **58**: 718–725.
8. **Rausch ME, Weisberg S, Vardhana P, Tortoriello DV.** 2008. Obesity in C57BL/6J mice is characterized by adipose tissue hypoxia and cytotoxic T-cell infiltration. Int. J. Obes. (Lond.) **32**:451–463.
9. **Ye J, Gao Z, Yin J, He Q.** 2007. Hypoxia is a potential risk factor for chronic inflammation and adiponectin reduction in adipose tissue of ob/ob and dietary obese mice. Am. J. Physiol. Endocrinol. Metab. **293**: E1118–E1128. doi:10.1152/ajpendo.00435.2007.
10. **Halberg N, Khan T, Trujillo ME, Wernstedt-Asterholm I, Attie AD, Sherwani S, Wang ZV, Landskroner-Eiger S, Dineen S, Magalang UJ, Brekken RA, Scherer PE.** 2009. Hypoxia-inducible factor 1alpha induces fibrosis and insulin resistance in white adipose tissue. Mol. Cell. Biol. **29**:4467–4483.
11. **Wang B, Wood IS, Trayhurn P.** 2007. Dysregulation of the expression and secretion of inflammation-related adipokines by hypoxia in human adipocytes. Pflugers Arch. **455**:479–492.
12. **Semenza GL.** 2000. Hypoxia, clonal selection, and the role of HIF-1 in tumor progression. Crit. Rev. Biochem. Mol. Biol. **35**:71–103.
13. **Rocha S.** 2007. Gene regulation under low oxygen: holding your breath for transcription. Trends Biochem. Sci. **32**:389–397.
14. **Kallio PJ, Wilson WJ, O'Brien S, Makino Y, Poellinger L.** 1999. Regulation of the hypoxia-inducible transcription factor 1alpha by the ubiquitin-proteasome pathway. J. Biol. Chem. **274**:6519–6525.
15. **Bruick RK, McKnight SL.** 2001. A conserved family of prolyl-4-hydroxylases that modify HIF. Science **294**:1337–1340.
16. **Ivan M, Kondo K, Yang H, Kim W, Valiando J, Ohh M, Salic A, Asara JM, Lane WS, Kaelin WG, Jr.** 2001. HIFalpha targeted for VHL-mediated destruction by proline hydroxylation: implications for O2 sensing. Science **292**:464–468.
17. **Salceda S, Caro J.** 1997. Hypoxia-inducible factor 1alpha (HIF-1alpha) protein is rapidly degraded by the ubiquitin-proteasome system under normoxic conditions. Its stabilization by hypoxia depends on redox-induced changes. J. Biol. Chem. **272**:22642–22647.
18. **Brahimi-Horn MC, Pouyssegur J.** 2007. Oxygen, a source of life and stress. FEBS Lett. **581**:3582–3591.
19. **Semenza GL.** 2003. Targeting HIF-1 for cancer therapy. Nat. Rev. Cancer **3**:721–732.
20. **Khan T, Muise ES, Iyengar P, Wang ZV, Chandalia M, Abate N, Zhang BB, Bonaldo P, Chua S, Scherer PE.** 2009. Metabolic dysregulation and adipose tissue fibrosis: role of collagen VI. Mol. Cell. Biol. **29**:1575–1591.
21. **Belozerov VE, Van Meir EG.** 2005. Hypoxia inducible factor-1: a novel target for cancer therapy. Anticancer Drugs **16**:901–909.
22. **Belozerov VE, Van Meir EG.** 2006. Inhibitors of hypoxia-inducible factor-1 signaling. Curr. Opin. Investig. Drugs **7**:1067–1076.
23. **Powis G, Kirkpatrick L.** 2004. Hypoxia inducible factor-1alpha as a cancer drug target. Mol. Cancer Ther. **3**:647–654.
24. **Sun X, Kanwar JR, Leung E, Lehnert K, Wang D, Krissansen GW.** 2001. Gene transfer of antisense hypoxia inducible factor-1 alpha enhances the therapeutic efficacy of cancer immunotherapy. Gene Ther. **8**:638–645.
25. **Welsh SJ, Powis G.** 2003. Hypoxia inducible factor as a cancer drug target. Curr. Cancer Drug Targets **3**:391–405.
26. **Welsh S, Williams R, Kirkpatrick L, Paine-Murrieta G, Powis G.** 2004. Antitumor activity and pharmacodynamic properties of PX-478, an inhibitor of hypoxia-inducible factor-1alpha. Mol. Cancer Ther. **3**:233–244.
27. **Jacoby JJ, Erez B, Korshunova MV, Williams RR, Furutani K, Takahashi O, Kirkpatrick L, Lippman SM, Powis G, O'Reilly MS, Herbst RS.** 2010. Treatment with HIF-1alpha antagonist PX-478 inhibits progression and spread of orthotopic human small cell lung cancer and lung adenocarcinoma in mice. J. Thorac. Oncol. **5**:940–949.
28. **Jordan BF, Black K, Robey IF, Runquist M, Powis G, Gillies RJ.** 2005. Metabolite changes in HT-29 xenograft tumors following HIF-1alpha inhibition with PX-478 as studied by MR spectroscopy in vivo and ex vivo. NMR Biomed. **18**:430–439.
29. **Koh MY, Spivak-Kroizman T, Venturini S, Welsh S, Williams RR, Kirkpatrick DL, Powis G.** 2008. Molecular mechanisms for the activity of PX-478, an antitumor inhibitor of the hypoxia-inducible factor-1alpha. Mol. Cancer Ther. **7**:90–100.
30. **Lee K, Kim HM.** 2011. A novel approach to cancer therapy using PX-478 as a HIF-1alpha inhibitor. Arch. Pharm. Res. **34**:1583–1585.
31. **Palayoor ST, Mitchell JB, Cerna D, Degraff W, John-Aryankalayil M, Coleman CN.** 2008. PX-478, an inhibitor of hypoxia-inducible factor-1alpha, enhances radiosensitivity of prostate carcinoma cells. Int. J. Cancer **123**:2430–2437.
32. **Schwartz DL, Bankson JA, Lemos R, Jr, Lai SY, Thittai AK, He Y, Hostetter G, Demeure MJ, Von Hoff DD, Powis G.** 2010. Radiosensitization and stromal imaging response correlates for the HIF-1 inhibitor PX-478 given with or without chemotherapy in pancreatic cancer. Mol. Cancer Ther. **9**:2057–2067.
33. **Schwartz DL, Powis G, Thitai-Kumar A, He Y, Bankson J, Williams R, Lemos R, Oh J, Volgin A, Soghomonyan S, Nishii R, Alauddin M, Mukhopadhay U, Peng Z, Bornmann W, Gelovani J.** 2009. The selective hypoxia inducible factor-1 inhibitor PX-478 provides in vivo radiosensitization through tumor stromal effects. Mol. Cancer Ther. **8**:947–958.
34. **Chen J, Zhao S, Nakada K, Kuge Y, Tamaki N, Okada F, Wang J, Shindo M, Higashino F, Takeda K, Asaka M, Katoh H, Sugiyama T, Hosokawa M, Kobayashi M.** 2003. Dominant-negative hypoxia-inducible factor-1 alpha reduces tumorigenicity of pancreatic cancer cells through the suppression of glucose metabolism. Am. J. Pathol. **162**:1283–1291.

35. **Halterman MW, Miller CC, Federoff HJ.** 1999. Hypoxia-inducible factor-1alpha mediates hypoxia-induced delayed neuronal death that involves p53. J. Neurosci. **19**:6818–6824.
36. **Kung AL, Wang S, Klco JM, Kaelin WG, Livingston DM.** 2000. Suppression of tumor growth through disruption of hypoxia-inducible transcription. Nat. Med. **6**:1335–1340.
37. **Ryan HE, Poloni M, McNulty W, Elson D, Gassmann M, Arbeit JM, Johnson RS.** 2000. Hypoxia-inducible factor-1alpha is a positive factor in solid tumor growth. Cancer Res. **60**:4010–4015.
38. **Rajala MW, Scherer PE.** 2003. Minireview: the adipocyte—at the crossroads of energy homeostasis, inflammation, and atherosclerosis. Endocrinology **144**:3765–3773.
39. **Wang ZV, Deng Y, Wang QA, Sun K, Scherer PE.** 2010. Identification and characterization of a promoter cassette conferring adipocyte-specific gene expression. Endocrinology **151**:2933–2939.
40. **Sun K, Asterholm IW, Kusminski CM, Bueno AC, Wang ZV, Pollard JW, Brekken RA, Scherer PE.** 2012. Dichotomous effects of VEGF-A on adipose tissue dysfunction. Proc. Natl. Acad. Sci. U. S. A. **109**:5874–5879.
41. **Vikram DS, Zweier JL, Kuppusamy P.** 2007. Methods for noninvasive imaging of tissue hypoxia. Antioxid. Redox Signal. **9**:1745–1756.
42. **Khan M, Kwiatkowski P, Rivera BK, Kuppusamy P.** 2010. Oxygen and oxygenation in stem-cell therapy for myocardial infarction. Life Sci. **87**: 269–274.
43. **Pandian RP, Parinandi NL, Ilangovan G, Zweier JL, Kuppusamy P.** 2003. Novel particulate spin probe for targeted determination of oxygen in cells and tissues. Free Radic. Biol. Med. **35**:1138–1148.
44. **Khan M, Mohan IK, Kutala VK, Kotha SR, Parinandi NL, Hamlin RL, Kuppusamy P.** 2009. Sulfaphenazole protects heart against ischemia-reperfusion injury and cardiac dysfunction by overexpression of iNOS, leading to enhancement of nitric oxide bioavailability and tissue oxygenation. Antioxid. Redox Signal. **11**:725–738.
45. **Halberg N, Schraw TD, Wang ZV, Kim JY, Yi J, Hamilton MP, Luby-Phelps K, Scherer PE.** 2009. Systemic fate of the adipocyte-derived factor adiponectin. Diabetes **58**:1961–1970.
46. **Wang B, Wood IS, Trayhurn P.** 2008. Hypoxia induces leptin gene expression and secretion in human preadipocytes: differential effects of hypoxia on adipokine expression by preadipocytes. J. Endocrinol. **198**: 127–134.
47. **Lin S, Thomas TC, Storlien LH, Huang XF.** 2000. Development of high fat diet-induced obesity and leptin resistance in C57Bl/6J mice. Int. J. Obes. Relat. Metab. Disord. **24**:639–646.
48. **Trayhurn P, Wood IS.** 2004. Adipokines: inflammation and the pleiotropic role of white adipose tissue. Br. J. Nutr. **92**:347–355.
49. **Jiang C, Qu A, Matsubara T, Chanturiya T, Jou W, Gavrilova O, Shah YM, Gonzalez FJ.** 2011. Disruption of hypoxia-inducible factor 1 in adipocytes improves insulin sensitivity and decreases adiposity in high-fat diet-fed mice. Diabetes **60**:2484–2495.
50. **Krishnan J, Danzer C, Simka T, Ukropec J, Walter KM, Kumpf S, Mirtschink P, Ukropcova B, Gasperikova D, Pedrazzini T, Krek W.** 2012. Dietary obesity-associated Hif1alpha activation in adipocytes restricts fatty acid oxidation and energy expenditure via suppression of the Sirt2-NAD+ system. Genes Dev. **26**:259–270.
51. **Giaccia A, Siim BG, Johnson RS.** 2003. HIF-1 as a target for drug development. Nat. Rev. Drug Discov. **2**:803–811.
52. **Jordan BF, Runquist M, Raghunand N, Baker A, Williams R, Kirkpatrick L, Powis G, Gillies RJ.** 2005. Dynamic contrast-enhanced and diffusion MRI show rapid and dramatic changes in tumor microenvironment in response to inhibition of HIF-1alpha using PX-478. Neoplasia **7**:475–485.
53. **Brennan AM, Mantzoros CS.** 2006. Drug insight: the role of leptin in human physiology and pathophysiology—emerging clinical applications. Nat. Clin. Pract. Endocrinol. Metab. **2**:318–327.
54. **Mason SD, Rundqvist H, Papandreou I, Duh R, McNulty WJ, Howlett RA, Olfert IM, Sundberg CJ, Denko NC, Poellinger L, Johnson RS.** 2007. HIF-1alpha in endurance training: suppression of oxidative metabolism. Am. J. Physiol. Regul. Integr. Comp. Physiol. **293**:R2059–R2069. doi:10.1152/ajpregu.00335.2007.
55. **Hotamisligil GS.** 2006. Inflammation and metabolic disorders. Nature **444**:860–867.
56. **Yudkin JS.** 2003. Adipose tissue, insulin action and vascular disease: inflammatory signals. Int. J. Obes. Relat. Metab. Disord. **27**(Suppl 3):S25–S28.
57. **Weisberg SP, McCann D, Desai M, Rosenbaum M, Leibel RL, Ferrante AW, Jr.** 2003. Obesity is associated with macrophage accumulation in adipose tissue. J. Clin. Invest. **112**:1796–1808.
58. **Xu H, Barnes GT, Yang Q, Tan G, Yang D, Chou CJ, Sole J, Nichols A, Ross JS, Tartaglia LA, Chen H.** 2003. Chronic inflammation in fat plays a crucial role in the development of obesity-related insulin resistance. J. Clin. Invest. **112**:1821–1830.
59. **Aragonés J, Schneider M, Van Geyte K, Fraisl P, Dresselaers T, Mazzone M, Dirkx R, Zacchigna S, Lemieux H, Jeoung NH, Lambrechts D, Bishop T, Lafuste P, Diez-Juan A, Harten SK, Van Noten P, De Bock K, Willam C, Tjwa M, Grosfeld A, Navet R, Moons L, Vandendriessche T, Deroose C, Wijeyekoon B, Nuyts J, Jordan B, Silasi-Mansat R, Lupu F, Dewerchin M, Pugh C, Salmon P, Mortelmans L, Gallez B, Gorus F, Buyse J, Sluse F, Harris RA, Gnaiger E, Hespel P, Van Hecke P, Schuit F, Van Veldhoven P, Ratcliffe P, Baes M, Maxwell P, Carmeliet P.** 2008. Deficiency or inhibition of oxygen sensor Phd1 induces hypoxia tolerance by reprogramming basal metabolism. Nat. Genet. **40**:170–180.
60. **Mason SD, Howlett RA, Kim MJ, Olfert IM, Hogan MC, McNulty W, Hickey RP, Wagner PD, Kahn CR, Giordano FJ, Johnson RS.** 2004. Loss of skeletal muscle HIF-1alpha results in altered exercise endurance. PLoS Biol. **2**:e288.
61. **Tajima T, Goda N, Fujiki N, Hishiki T, Nishiyama Y, Senoo-Matsuda N, Shimazu M, Soga T, Yoshimura Y, Johnson RS, Suematsu M.** 2009. HIF-1alpha is necessary to support gluconeogenesis during liver regeneration. Biochem. Biophys. Res. Commun. **387**:789–794.
62. **Kabon B, Nagele A, Reddy D, Eagon C, Fleshman JW, Sessler DI, Kurz A.** 2004. Obesity decreases perioperative tissue oxygenation. Anesthesiology **100**:274–280.
63. **Virtanen KA, Lonnroth P, Parkkola R, Peltoniemi P, Asola M, Viljanen T, Tolvanen T, Knuuti J, Ronnemaa T, Huupponen R, Nuutila P.** 2002. Glucose uptake and perfusion in subcutaneous and visceral adipose tissue during insulin stimulation in nonobese and obese humans. J. Clin. Endocrinol. Metab. **87**:3902–3910.
64. **Abrosini G, Nath AK, Sierra-Honigmann MR, Flores-Riveros J.** 2002. Transcriptional activation of the human leptin gene in response to hypoxia: involvement of hypoxia-inducible factor 1. J. Biol. Chem. **277**: 34601–34609.